16th World Conference on Earthquake, 16WCEE 2017

Santiago Chile, January 9th to 13th 2017

Paper N° 1928 (Abstract ID)

Registration Code: S-W1461750543

BEHAVIOUR OF NON AND PARTIALLY RE-CENTERING STRUCTURES UNDER REPEATED GROUND MOTIONS

G. Rinaldin[(1)], L. Scaramuzza[(2)], C. Amadio[(3)], M. Fragiacomo[(4)]

[(1)] *Post-doc research fellow, University of Sassari, grinaldin@uniss.it*
[(2)] *MSc student, University of Trieste, scaramuzza_lorenzo@libero.it*
[(3)] *Full professor, University of Trieste, amadio@units.it*
[(4)] *Full professor, University of L'Aquila, massimo.fragiacomo@univaq.it*

Abstract

The self-centering capacity of a structure after a seismic event is an important feature of a well-designed seismic-resistant building. For this reason, self-centering isolators and/or dampers systems have been widely used recently to ensure this behavior in structures built in earthquake-prone areas. Another main issue related to a good seismic design is the resilience of the building when subjected to a seismic sequence, which may cause a significant accumulation of damage and the loss of the structure.

In this work, the effect of repeated ground motions on structures with different hysteretic behavior is studied using non-linear Single Degree of Freedom (SDOF) systems. Extensive dynamic analyses were carried out for natural ground motion sequences, namely sequences of more than one natural seismic record. Systems with different dissipative hysteretic laws, linear and non-linear damping behavior were considered with the aim to emphasize the difference in cumulated damage and seismic response. In addition, the re-centering capability of the structures after a ground motion was analyzed since hysteresis behaviors with strong post-earthquake residual deformations may lead to downtime and an unacceptable condition for the building. Some simple design rules for buildings in seismic areas subjected to repeated earthquakes are finally given.

Keywords: Re-centering structures, Repeated ground motions, SDOF, Non-linear damping, Hysteretic behavior

1. Introduction

The self-centering capacity of a structure after a seismic event is an important feature of a well-designed seismic-resistant building. In the last years, self-centering isolators and/or dampers were extensively used to ensure this behavior in structures built in earthquake-prone areas [1], [2], [3]. Another main issue related to a good seismic design is the resilience of the building when subjected to a seismic sequence that may cause the loss of the building due to cumulated damage [4]. In steel buildings, studied for example in [1] and [4], the residual deformations after a seismic event (e.g. the mainshock in a sequence) strongly influence the response of the aftershocks, in particular when they have the same or a greater Peak Ground Acceleration (PGA) [5].

In general, structural design should always be carried out in accordance with the concept of resilience [6]. The resilience of a system is its capacity to revert to a fully operational state after an event that interrupted temporarily its functionality. Resilience in structural engineering can be achieved with robustness and redundancy of the structure, which are respectively the ability to avoid disproportionate damage (collapse for example) in the case in which the structure undergoes local serious damage, and the duplication of the critical components of a structure with the intention of increasing its reliability and availability. Professional engineers can choose either to design a more robust structure or, as suggested by the current codes of practice such as [7], accepting a damage in the structure, which must be controlled with plasticization in some selected parts, or equipping the building with devices (e.g. dampers, isolators) to absorb the seismic input energy instead of the structure [8]. In general, it is economically more convenient to adopt one of the two last options (dampers, isolators), especially when the building has to be designed to withstand the maximum expected earthquake.

In this paper, the effect of repeated ground motions on structures with different hysteretic behavior is investigated using Single Degree of Freedom (SDOF) systems, which schematize the base shear capacity and cyclic behavior of entire buildings, in accordance with the N2 method [9].

Extensive dynamic analyses were carried out for some ground motion sequences, namely sequences of more than one natural seismic record. The fully dissipative hysteretic law, typical of non recentering structures, was employed to investigate the requested ductility level and to estimate the inelastic spectra, including information on the residual damage after the seismic sequence. Furthermore, non-linear dampers and recentering SDOF systems were analyzed, with the aim to study their behavior under a seismic sequence. Simple design rules for dissipative non recentering structures are also introduced. To obtain inelastic spectra, the software OpenSees [10] was employed.

2. Selected seismic sequences

The selection of appropriate seismic sequences is a fundamental aspect in this research. Not all the sequences composed by mainshock and aftershock are significant and worth of consideration in this study. Natural seismic records were selected on the basis of their peak ground acceleration (PGA), and taken from the NIED [11], COSMOS [12] and ITACA [13] online databases.

The PGA of an earthquake directly affects the maximum drift of a structure and, if yielding occurs, the maximum ductility level required by the considered ground motion. Aftershock records must therefore be selected with an equal or greater PGA than the mainshock. The magnitude of the earthquake does not markedly affect the required level of ductility [14], as will be also shown in this paper.

Table 1 presents all the main characteristics of the selected natural ground motion sequences. Each record was assembled in a single time-history sequence, placing a zero acceleration plateau for a duration of at least 30s between two consecutive records. This plateau permits the SDOF to return in a state of rest before the subsequent record starts. In this paper, three sequences are investigated in detail: Christchurch 2010-2011, Nocera Umbra 1997 and Niigata 2004, whose sequences and elastic spectra are depicted in Figs. 1 to 3.

Based on the analyses carried out, the seismic sequences used in this paper have been subdivided into three groups (see Table 1):

A. The ductility requested by one ground motions is almost the same as the one of the entire sequence. Hence, all the other records in the sequence have a lower spectrum, in the range [0;4s] (i.e. the Christchurch sequence);

Table 1 – Characteristics of considered seismic sequences

Group	Sequence	Date	Station name	Mw	Direction [N-S=0°]	PGA	Epicentral distance	Focal depth	Duration
						[m/s^2]	[km]	[km]	[s]
A	Christchurch	03/09/2010 16:35	CBGS	7.1	0°	-1.5101	36	10	110
		21/02/2011 23:51	CBGS	6.1	0°	5.5627	9.6	5.9	110
B	Nocera Umbra	10/06/1997 23:24	NCR	5.4	0°	-4.8129	11.1	5.5	37
		26/09/1997 00:33	NCR	5.7	0°	4.8588	13.2	5.7	29
		26/09/1997 09:40	NCR	6	0°	-4.9217	10.9	5.7	14
B	Mexicali Valley	11/03/1978 05:40	VCTRA	3.7	135°	4.5915	16	5.6	13
		11/03/1978 23:57	VCTRA	4.8	135°	4.578	2	6	10
		12/03/1978 00:30	VCTRA	4.5	135°	-4.515	7	6	12
B	Mendocino Cape	25/04/1992 11:06	Petrolia CA	7	0°	-5.7813	15.9	9.6	60
		26/04/1992 00:41	Petrolia CA	6.6	0°	5.8723	35.1	20	40
C	Chi Chi, Taiwan	20/09/1999 17:47	TCU129	7.6	90°	-9.8393	2.2	6.8	160
		20/09/1999 18:03	TCU129	6.2	90°	-9.3302	12.8	8	104
C	Niigata	23/10/2004 17:56	NIG020	6.6	0°	-5.2143	23.2	15.8	299
		23/10/2004 18:34	NIG020	6.3	0°	-5.2662	27.8	22.2	299
		25/10/2004 06:05	NIG020	5.7	0°	-4.2706	35.7	16.7	299
		27/10/2004 10:40	NIG020	6	0°	-5.231	18.8	15.7	299
C	NWChina	05/04/1997 23:46	Jiashi	5.9	270°	-2.2931	26.6	23.1	45
		11/04/1997 05:34	Jiashi	6.1	270°	2.685	27.7	20	60
		15/04/1997 18:19	Jiashi	5.8	270°	2.3451	33.6	22.4	60
C	Tohoku	11/03/2011 14:46	MYG001	9	0	4.1266	101	29	300
		07/04/2011 23:32	MYG001	7.1	0	3.8982	81.2	42	184
C	Hokkaido	29/11/2004 03:32	HKD071	7	0	2.7214	52.8	43.8	159
		06/12/2004 23:15	HKD071	6.7	0	2.9398	51.8	35.8	121
C	Weber	19/02/1990 05:34	120A	6.2	102°	1.4426	38	24.2	51
		13/05/1990 04:23	120A	6.4	102°	1.6475	33	12	54

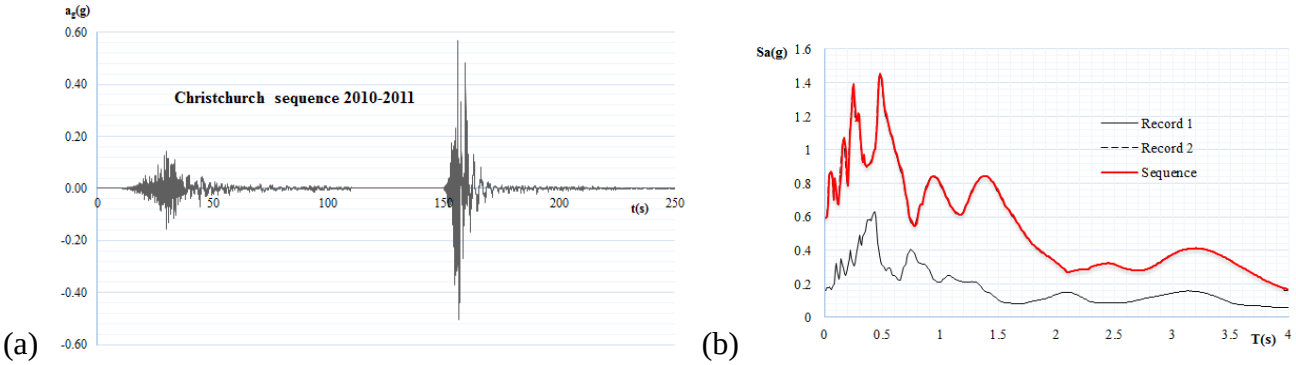

(a) (b)

Fig. 1 – Christchurch seismic sequence: acceleration time-history (a) and pseudo-acceleration elastic spectra (b)

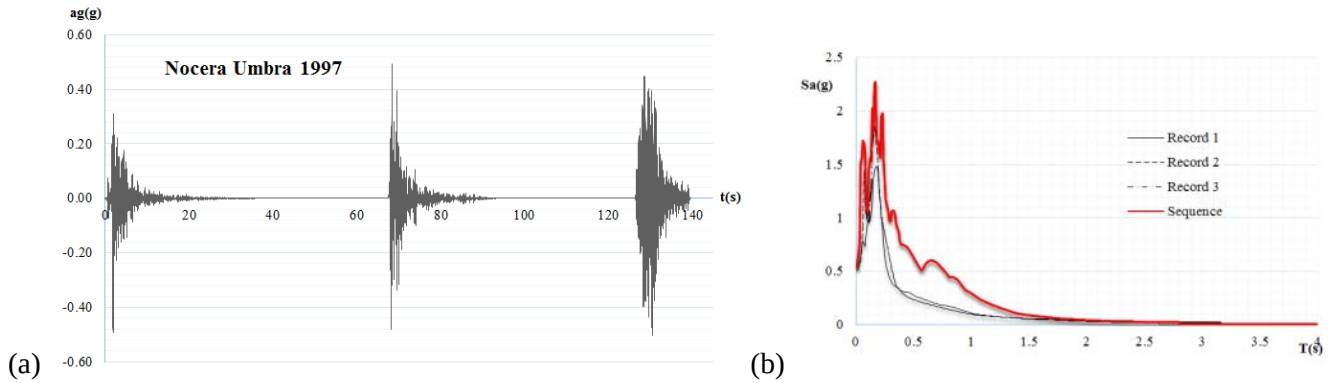

(a) (b)

Fig. 2 – Nocera Umbra seismic sequence: acceleration time-history (a); pseudo-acceleration elastic spectra (b)

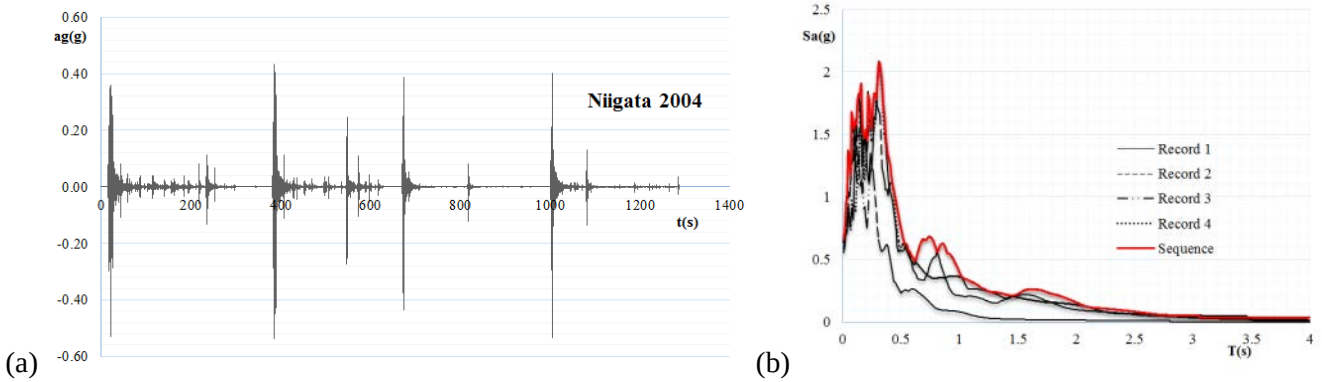

(a) (b)

Fig. 3 – Niigata seismic sequence: acceleration time-history (a) and pseudo-acceleration elastic spectra (b)

B. The ductility requested by the sequence is different from that of the single ground motions over the entire range of periods considered (i.e. Nocera Umbra sequence);

C. The ductility requested by the sequence is different from that of single ground motions over a limited period range (i.e. Niigata sequence).

3. Numerical analyses

A purposely-developed program, written in Fortran, has been used to obtain the inelastic spectra of the seismic sequences. The program performs a dynamic analysis using the Newmark beta-method, assuming constant acceleration for each step. Elasto-plastic with no hardening (EPP – Fig. 4a) and bilinear hysteretic laws with stiffness of the hardening phase set to 10% of the elastic one (EP10 – Fig. 4b) have been considered in the analyses.

The software provides as an output the inelastic spectrum for a constant ductility by changing the values of yield force F_y which leads to the desired level of ductility. After an initial scanning, the program uses the bisection method displayed in Fig. 5. Finally, the maximum absolute acceleration for each natural vibration period is collected.

A second purposely-written software has been developed to estimate the required ductility for each seismic sequence. The yield force F_y is determined for each analyzed SDOF according to Eq. (1) by multiplying the elastic spectral acceleration at a certain natural vibration period T by a reduction factor k, which has been set to 0.3, 0.5 and 0.7, with the aim to consider different strength levels of the structure.

$$F_y = S_{a,elastic}(T_i) \cdot \mathrm{m} \cdot \mathrm{k} \tag{1}$$

with m the unitary mass and k the aforementioned reduction factor.

The nonlinear dynamic analyses have been carried out for the entire seismic sequence. The ductility levels investigated are 2 and 6, and a constant damping ratio of 0.05 has been used for all cases.

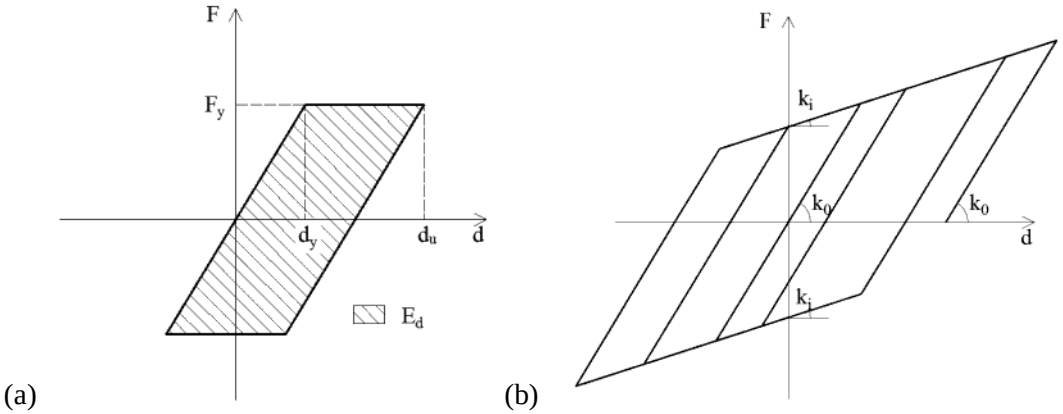

Fig. 4 – Elasto-plastic (EPP) (a) and bilinear (EP10) hysteretic law with 10% hardening

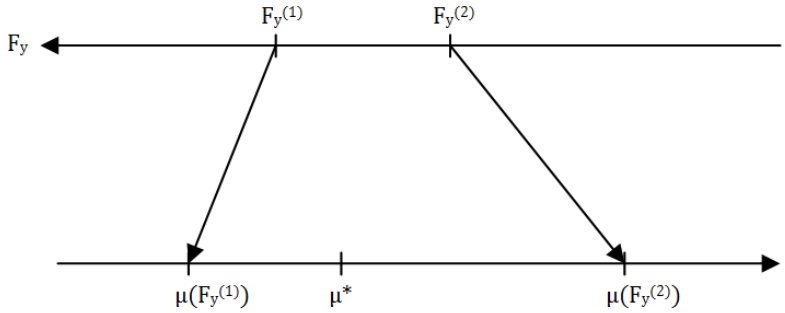

Fig. 5 – Bisection method used in the purposely-developed software

The results for the aforementioned seismic sequences are representative of a non-recentering structure as the hysteretic laws of the most common structural systems (steel, concrete and timber) are generally characterized by a non-recentering behavior. Only in few cases the structure can re-centers after a seismic event [15].

In this paper, a possible solution for dissipating the seismic input energy and re-center the structures after an event is investigated. The solution is made of nonlinear dampers used together with a spring of appropriate stiffness, which is typically represented by the connected structure. Such a possible solution has been investigated using the OpenSees framework [10], which allows the user to carry out dynamic analyses on a nonlinear damper assembled in the SDOF structure as depicted in Fig. 6. Here, the dashpot is modelled using the Maxwell's model (spring and damper in series).

The system displayed in Fig. 6 behaves according to Eq. (2),

$$F = c_{NL}\dot{d}^{\alpha} + K_s d + F_0 \tag{2}$$

where F signifies the total force in the SDOF, c_{NL} is the non-linear damping coefficient, $\alpha<1$ is the damping exponent, $\dot{d}$ denotes the mass velocity, d the mass displacement, F_0 the friction force, modelled with a rigid-plastic spring usually provided in commercial damping devices, K_s the elastic stiffness of the device for the recentering and K_d a high stiffness proper of the fluid that composes the device.

Features like the nonlinear damping and the friction spring have been introduced with the aim to maximize the energy dissipation. Such model has been employed in the following cases:

i. with linear damping ($\alpha=1$ and $c_{NL} = c_L = 2\omega\xi m$, with damping ratio $\xi = 0.2$, typical of rubber bearing devices) and without friction spring;

ii. with nonlinear damping (α=0.35 and $\xi = 0.3$) and without friction spring, estimating the damping coefficient from the maximum displacement $S_{d,lin}$ obtained from a linear analysis, according to Eq. (3) [16]:

$$c_{NL} \cong c_L (0.8\omega S_{d,lin})^{1-\alpha} \quad (3)$$

iii. like case ii, but with the friction spring.

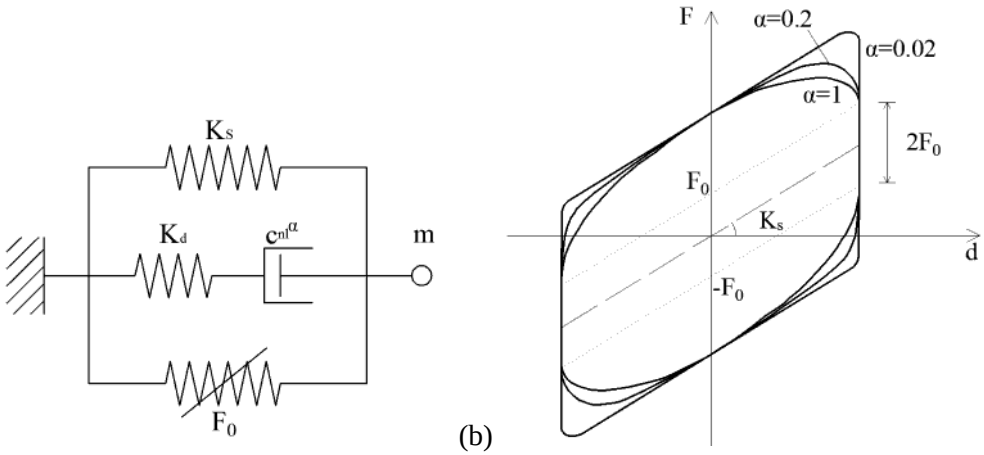

(a) (b)

Fig. 6 – Spring assembly in OpenSees (a) and force-displacement relationship for non-linear dampers with different damping exponents α<1 (b)

The studied SDOFs are representative of the structures depicted in Fig. 7. In case (a), the restoring forces to avoid any residual deformation after a seismic event are directly provided by the dampers mounted in the bracings, while in the case (b) the restoring force is given by the structure itself due to the elastic force developed by the semi-rigid joints of stiffness K_{str}. In both cases, the period of the structure is directly tied to stiffness K_s or K_{str} respectively.

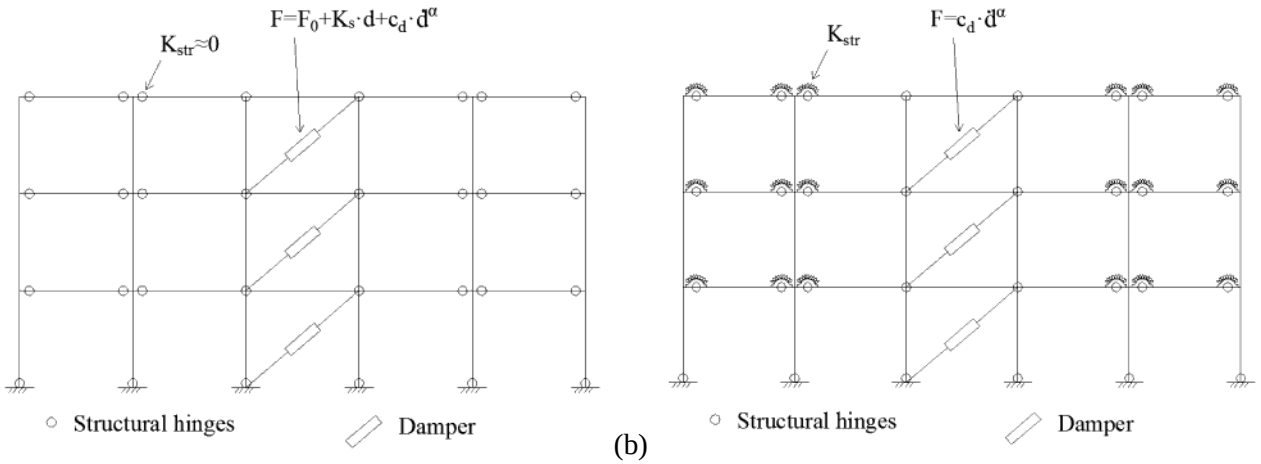

(a) (b)

Fig. 7 – Structures equipped with dampers: the restoring force is given by the dampers (a) or by the structure itself (b)

4. Non-recentering structures

Results in terms of inelastic spectra for the non-recentering systems (i.e. SDOF with EPP and EP10 behavior) are displayed in Figs. 8 and 9, respectively.

As can be noticed from the inelastic spectra, in the Christchurch sequence the dominant record (the second one) fully determines the envelope spectrum. Figure 10 displays the required ductility μ_r for the EPP and EP10 systems assuming k=0.3.

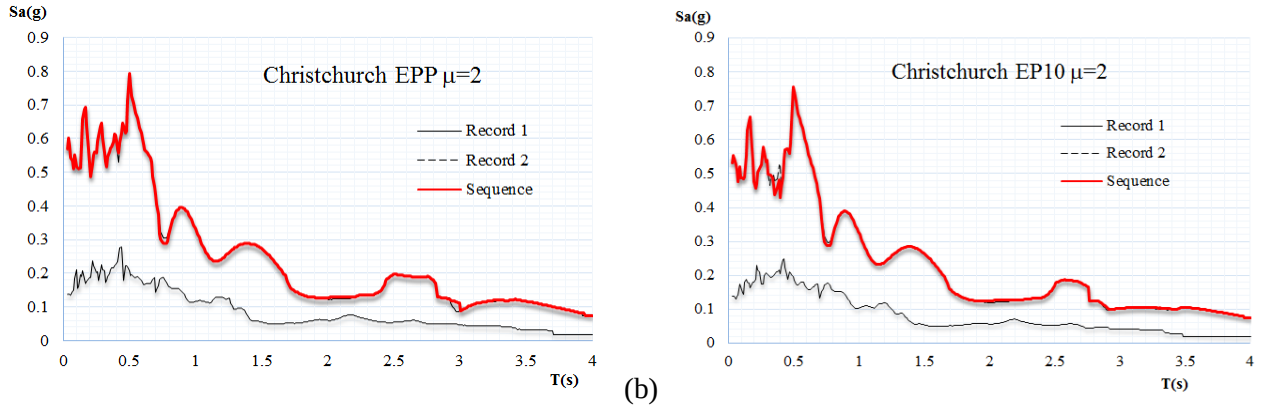

(a) (b)

Fig. 8 – Inelastic spectra for the EPP (a) and EP10 (b) systems with ductility 2 for the Christchurch sequence

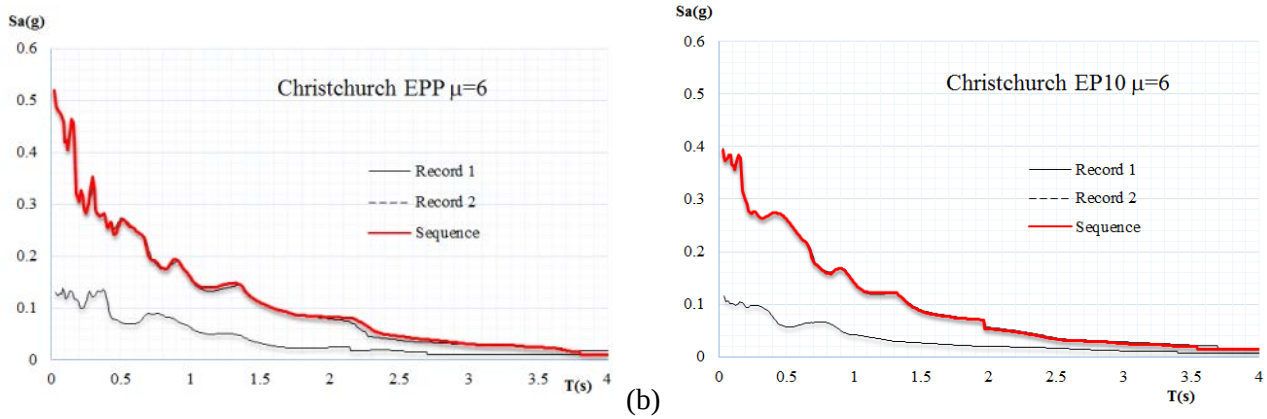

(a) (b)

Fig. 9 – Inelastic spectra for the EPP (a) and EP10 (b) systems with ductility 6 for the Christchurch sequence

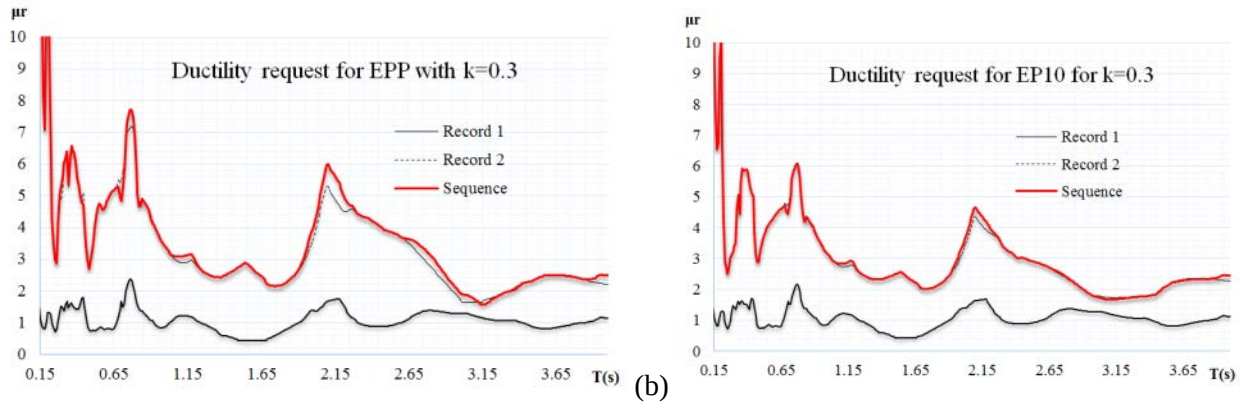

(a) (b)

Fig. 10 – Required ductility for the EPP (a) and EP10 (b) systems for the Christchurch sequence

The Nocera Umbra sequence, for which the inelastic spectra are presented in Fig. 11, exhibits a slightly different behavior: a different ductility request of a single record with respect to the entire sequence can be noticed, as shown in Fig. 12.

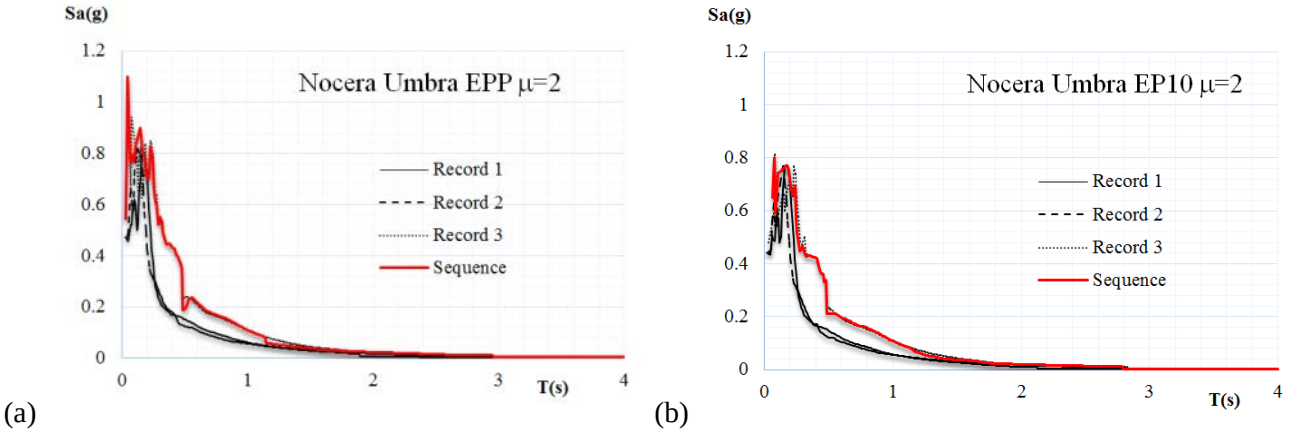

Fig. 11 – Inelastic spectra for the EPP (a) and EP10 (b) systems with ductility 2 for the Nocera Umbra sequence

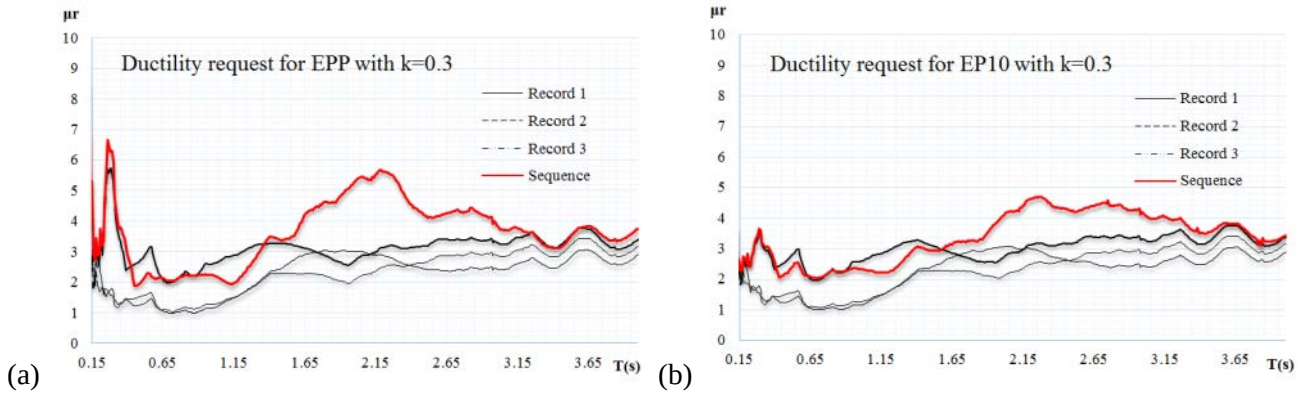

Fig. 12 – Required ductility for the EPP (a) and EP10 (b) systems for the Nocera Umbra sequence

Finally, the ductility requests from Niigata sequence are presented in Fig. 13. As can be clearly seen, for almost the entire period range (0;4s) the ductility required by the sequence is different from the one for each single record.

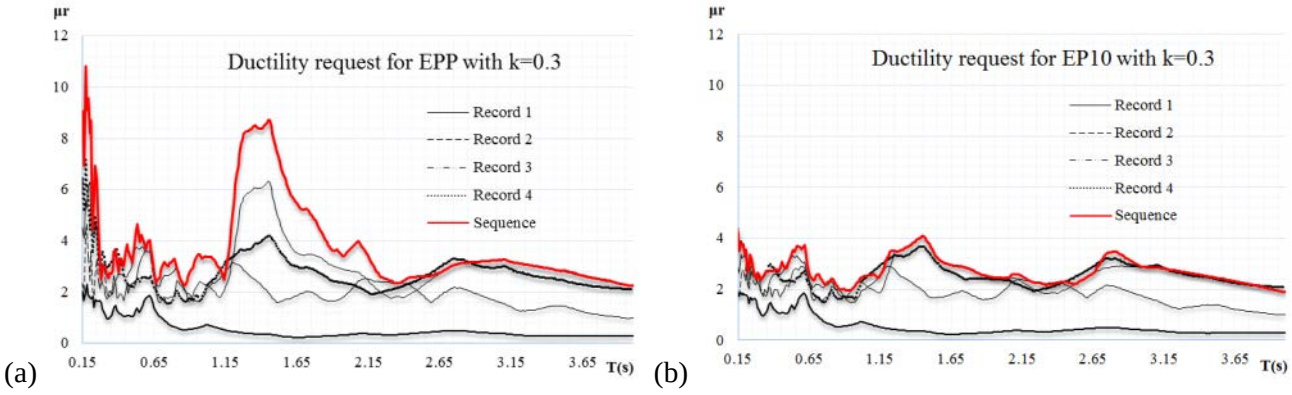

Fig. 13 – Required ductility for the EPP (a) and EP10 (b) systems for the Niigata sequence

The ductility requests have been collected for all the 10 seismic sequences listed in Table 1. With the aim to draw general conclusions, the ratio between the ductility demand by the sequence $\mu_{r,seq}$ and the envelope of the ones by each single event has been calculated for all the sequences in Table 1. Such ratio is defined as in Eq. (4),

$$R_\mu(\mathrm{T}) = \frac{\mu_{r,seq}}{\mu_{r,env}} \tag{4}$$

with $\mu_{r,env}$ signifying the envelope of the ductility requested by a single event of a sequence, for each natural vibration period *T*. Figure 14 shows the ratios calculated for all sequences, and the 95% percentile of all curves.

Moreover, the behavior factor *q* has been calculated according to Eq. (5),

$$q = \frac{F_e}{F_y} = \frac{S_{a,el}(\mathrm{T})}{F_y(\mathrm{T})} \tag{5}$$

being $S_{a,el}(\mathrm{T})$ the pseudo-acceleration given by the elastic spectrum for the period *T*, and $F_y(\mathrm{T})$ the corresponding force at the elastic limit, collected calculating the inelastic spectra. Such ratio has been evaluated for each sequence and for each single event, as depicted in Fig. 14.

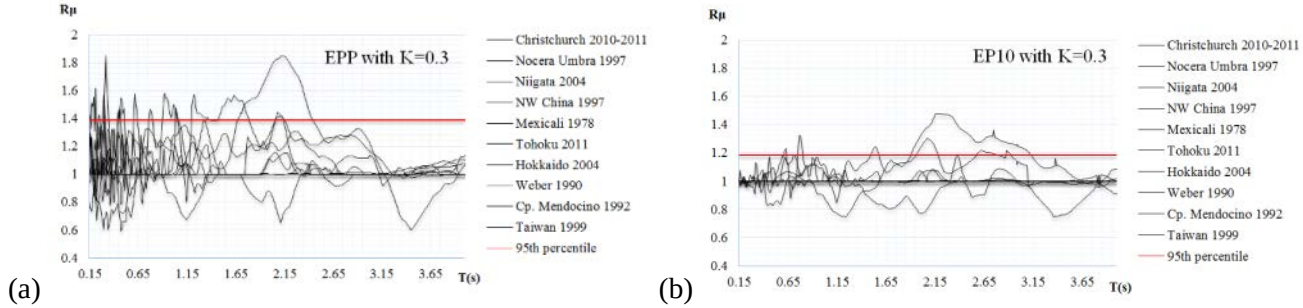

(a) (b)

Fig. 14 – Ductility ratios for the EPP (a) and EP10 (b) systems, for all sequences

Finally, the ratio between the behavior factor for each natural vibration period can be expressed as in Eq. (6a),

$$R_q(T) = \frac{q_{seq}}{q_{env}} \tag{6a}$$

$$R_q(T) = \frac{\dfrac{F_{e,seq}}{F_{y,seq}}}{\max\dfrac{F_{e,env}}{F_{y,env}}} \cong \frac{\dfrac{F_{e,seq}}{F_{y,seq}}}{\dfrac{\max(F_{e,env})}{\max(F_{y,env})}} = \frac{\max(F_{y,env})}{F_{y,seq}} \cong \frac{1}{R_\mu(T)} \tag{6b}$$

with q_{seq} the behavior factor for the sequence and q_{env} the envelope of the behavior factors for each single record. This ratio is almost equal to the inverse of the ductility ratio $R_\mu(T)$, accepting the approximation that $q = \mu$ for all the periods, even the shortest ones (Eq. 6b). Fig. 15 presents the R_q values for all sequences, including their 5th percentile.

As a result, a reduction for the *q* factor usually employed for structures with the same hysteretic behavior under a single earthquake ground motion can be proposed adopting for R_q the 5th percentile. Such a reduction can be set as in Table 2. Table 3 shows the proposed increase of the structural ductility, on the basis of the R_μ ratios calculated earlier. As can be seen from the data reported, the reduction proposed for the behavior factor *q* for $\mu=2$ corresponds to the inverse of the ductility increase in Table 3 for *k=0.5*, confirming the reciprocal relationship between R_q and R_μ expressed by Eq. (6b).

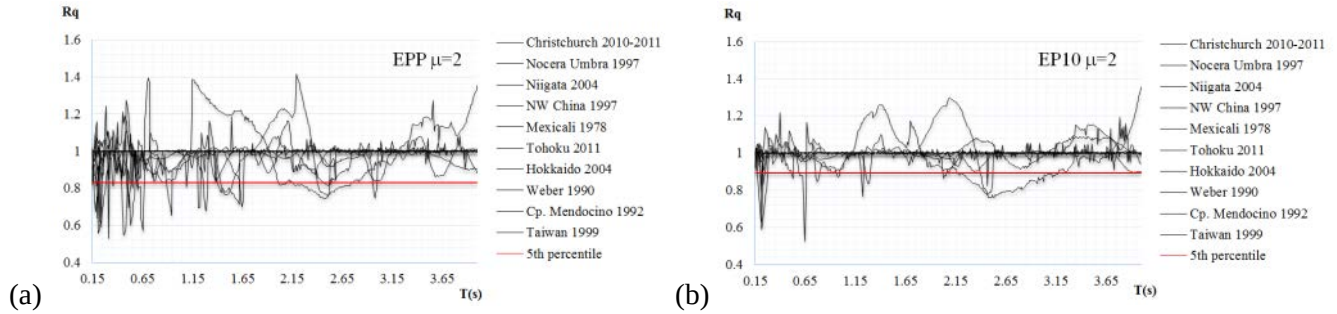

(a) (b)

Fig. 15 – Behavior factor ratios for the EPP (a) and EP10 (b) systems, for all seismic sequences

Table 2 – Proposed reduction of behavior factor R_q

	5th percentile		*q reduction*	
Behavior	**μ=2**	μ=6	**μ=2**	μ=6
EPP	**0.83**	0.67	**-17%**	-33%
EP10	**0.89**	0.85	**-11%**	-15%

Table 3 – Proposed increased in ductility R_μ

	95th percentile of Rμ			*Increase in ductility*		
Behavior	k=0.3	**k=0.5**	k=0.7	k=0.3	**k=0.5**	k=0.7
EPP	1.39	**1.22**	1.15	39%	**22%**	15%
EP10	1.18	**1.13**	1.11	18%	**13%**	11%

5. Structures with dampers

The three investigated families of dampers were chosen with the aim to cover the most common design cases: (i) linear viscous dampers (called VL) representative of rubber bearing devices, (ii) non-linear viscous dampers (VNL) designed on the basis of the ultimate displacement obtained from the linear analysis, (iii) viscous non-linear dampers with friction effect (VNLF), designed like for the VNL systems. In all nonlinear cases ((ii) and (iii)), the damping exponent has been set to $\alpha=0.35$.

The different cyclic behaviors are depicted in Fig. 16a, where the time history response of the SDOF structure is plotted at $T=1s$ for the Nocera Umbra sequence. It has to be noticed how the friction effect can reduce the maximum displacement with a wider dissipating cycle.

Results from Niigata sequence are presented afterwards, in terms of absolute acceleration A vs. the period T. For the linear damper with a damping ratio of 20% (typical of a rubber bearing device), the damped spectra are presented in Fig. 16b. It can be noticed how, also in all the subsequent cases, the damped spectra for the sequence is always the envelope of the record composing the sequence itself.

The same linear analysis has been conducted with a damping coefficient of 30% with the aim to find out the maximum elastic displacement and calculate the nonlinear damping coefficient like in Eq. (3). For each natural vibration period T, the damped spectra are presented in Fig. 17a. The first two types of dampers underwent a complete recentering after each seismic event in the sequence. Finally, the same investigation has been conducted with the friction effect, represented with a rigid-perfectly plastic behavior set to 15% of the maximum force required from the elastic analysis. The results, displayed in Fig. 17b, demonstrate lower accelerations, especially for short natural vibration periods. Conversely, this type of dampers can present a limited, residual deformation due to the friction effect introduced. In this case the recentering stops when the damper is in a state of equilibrium with the friction force.

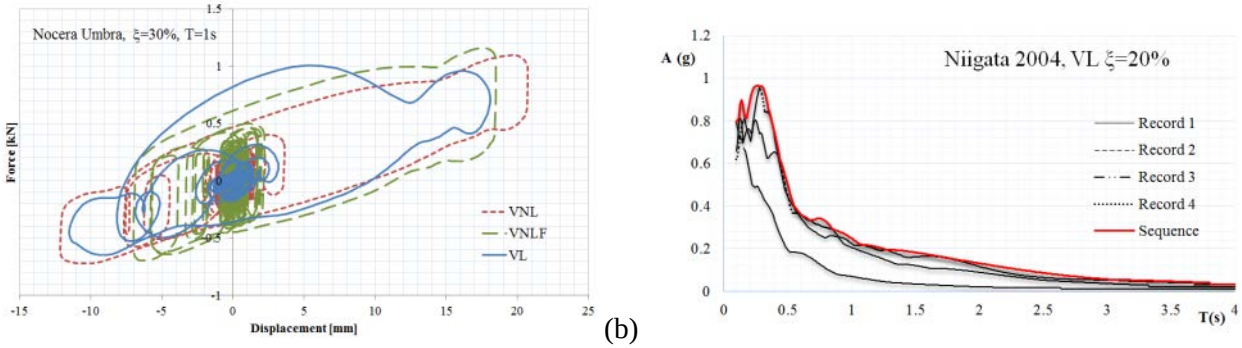

(a) (b)

Fig. 16 – Different behaviors of the employed damping models (a) and linear damped spectra for Niigata sequence (b)

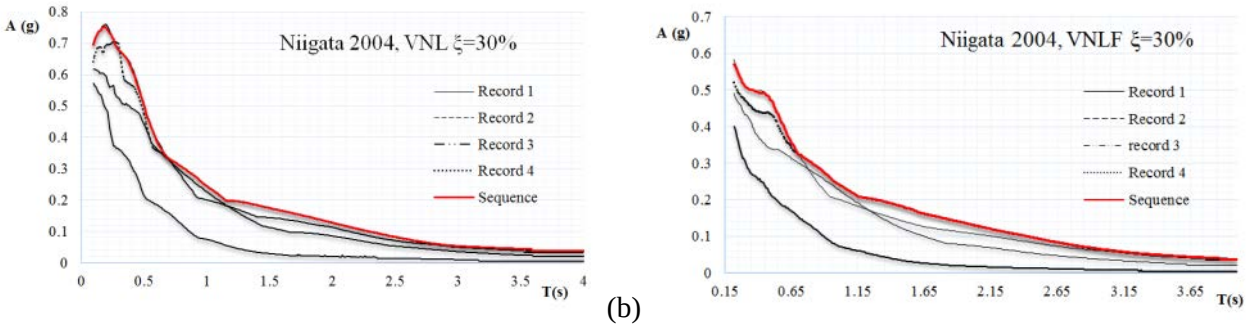

(a) (b)

Fig. 17 – Nonlinear damped spectra for Niigata sequence without (a) and with friction effect (b)

6. Conclusions

In this work, inelastic spectra of non- and recentering structures have been drawn for a series of natural sequences through non-linear dynamic analyses performed on SDOF systems. Firstly, a full dissipative hysteresis law has been presented to obtain inelastic spectra for 10 well-known natural seismic sequences, taken from literature. Results have been collected for systems with elasto-plastic behavior or with bilinear behavior an 10% of plastic hardening. As can be seen from the presented plots, the ductility requested by the seismic sequence to the structure can increase from 11 to 39%, due to the cumulated damage. Conversely, a reduction in the behavior factor has been found to be in the range 11 to 17% for a ductility level of 2 and in the range 15 and 33% for a ductility level of 6. This reduction should therefore be considered in earthquake prone areas characterized by seismic sequences.

An efficient way to improve structural resilience under a seismic sequence was shown to equip a building with dampers, which dissipate the seismic input energy in a viscous form, coupled with an elastic spring system, so as to help recentering. Dynamic nonlinear analyses conducted for three different configurations: with linear, nonlinear and nonlinear with friction dampers were presented. The results confirm that not only is the spectral acceleration lower due to the high damping ratio (from 20 to 30%), but also the maximum displacements are lower for each period *T*, as displayed in Fig. 18 for the Nocera Umbra sequence.

Analogous results were obtained for all the analyzed sequences where the spectra of the sequence were nearly coincident with the envelope spectra of single events without an accumulation of damage. Furthermore, if dampers are employed, the cumulated damage is considerably lower, and the structure demonstrates a recentering capacity after the event. Nonlinear dampers with friction effect cannot perform a full recentering due to the friction force that prevent the revert in a zero-deformation state but they are very efficient systems. The proposed strategy should be investigated more in deep, in particular for the automatic recentering structures having a flag-shaped hysteresis cycle [14], to draw general conclusions.

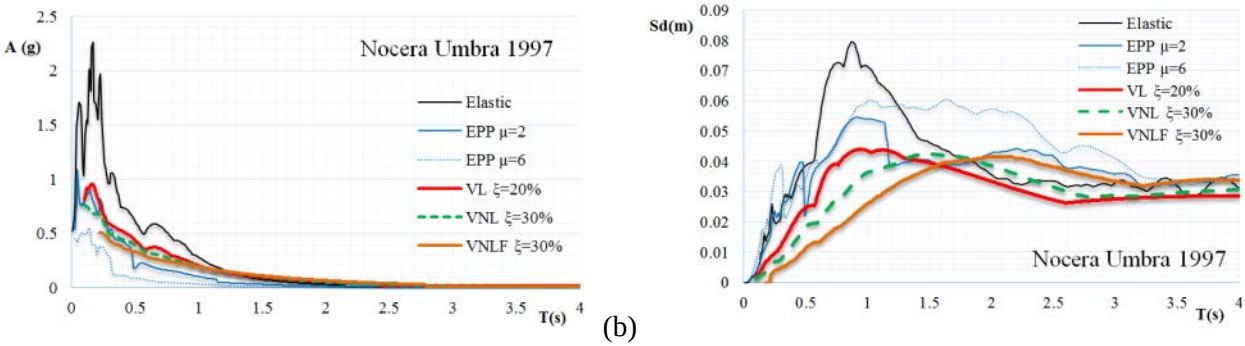

(a) (b)

Fig. 18 – Nonlinear damped spectra for Nocera Umbra sequence in terms of absolute acceleration (a) and displacement (b)

References

[1] Rad AA, MacRae GA, Yeow TZ, Bull D (2015): Earthquake sequence effect on steel building, *Proceedings of 8th* International Conference on Behavior of Steel Structures in Seismic Areas, Shangai, China, July 1-3.

[2] Dolce M, Cardone D, Marnetto R (2001): SMA Re-centering Devices for Seismic Isolation of Civil Structures, *Proceedings of SPIE*, Vol. 4330, 2001 SPIE 0277-786X/01, 238-249.

[3] Sancin L, Rinaldin G, Fragiacomo M, Amadio C (2014): Seismic analysis of an isolated and a non-isolated light-frame timber building using artificial and natural accelerograms, *Bollettino di Geofisica Teorica e Applicata - An International Journal of Earth Sciences*, **55**, 1, 103-118.

[4] Fragiacomo M, Amadio C, Macorini L (2004): Seismic response of steel frames under repeated earthquake ground motions, *Engineering Structures*, **26**, 2021–2035, 2004.

[5] Amadio C, Fragiacomo M, Rajgelj S. (2003): The effects of repeated earthquake ground motions on the non-linear response of SDOF systems. *Earthquake engineering & structural dynamics*, **32** (2), 291-308.

[6] Bruneau M, Reinhorn A (2006): Overview of the Resilience Concept. Proceedings of the 8th U.S. National Conference on Earthquake Engineering, 2040, April 18-22, 2006, San Francisco, California, USA.

[7] CEN, European Committee for Standardisation (2005): Eurocode 8, 2005. Design of structures for earthquake resistance - Part 1, General rules, seismic actions and rules for buildings. EN 1998-1:2005.

[8] Poh'sie HG, Chisari C, Rinaldin G, Fragiacomo M, Amadio C, Ceccotti A (2015): Application of a Translational Tuned Mass Damper Designed by Means of Genetic Algorithms on a Multistory Cross-Laminated Timber Building. *Journal of Structural Engineering*, DOI: 10.1061/(ASCE)ST.1943-541X.0001342

[9] Fajfar P (2000): A nonlinear analysis method for performance based seismic design. *Earthq Spectra*, **16** (3), 573–92.

[10] McKenna F. (2011): OpenSees: a framework for earthquake engineering simulation. Comput Sci Eng, **13** (4), 58–66.

[11] NIED - National Research Institute for Earth Science and Disaster Prevention, Database of the Strong-Motion Seismograph Networks (K-NET, KiK-net), Internet site: www.kyoshin.bosai.go.jp

[12] COSMOS. Strong Motion Data Center, Internet site: strongmotioncenter.org.

[13] Luzi L, Hailemikael S, Bindi D, Pacor F, Mele, F, Sabetta F (2008): ITACA (ITalian ACcelerometric Archive): A Web Portal for the Dissemination of Italian Strong-motion Data, *Seismological Research Letters*, **79** (5), 716–722. Doi: 10.1785/gssrl.79.5.716

[14] Amadio C, Rinaldin G, Fragiacomo G (2016): Investigation on the accuracy of the N2 method and the equivalent linearization procedure for different hysteretic models, *Soil Dynamics and Earthquake Engineering*, 69-80, DOI: 10.1016/j.soildyn.2016.01.005

[15] Buchanan A, Deam B, Fragiacomo M, Pampanin S, Palermo A. (2008): Multi-storey prestressed timber buildings in New Zealand. *Structural Engineering International, IABSE, Special Edition on Tall Timber Buildings*, **18** (2), 166-173.

[16] Silvestri S, Gasparini G, Trombetti T. (2010): A Five-Step Procedure for the Dimensioning of Viscous Dampers to Be Inserted in Building Structures. *Journal of Earthquake Engineering*, **14** (3), 417-447, DOI: 10.1080/13632460903093891.